Journal of Radiation Research, Vol. 60, No. 3, 2019, pp. 335–341
doi: 10.1093/jrr/rry111
Advance Access Publication: 22 January 2019

MRI response of obturator internus muscle to carbon-ion dose in prostate cancer treatment

Masahiro Kawahara[1,2,*], Hidemasa Kawamura[2], Yoshiki Kubota[2], Hiroyuki Katoh[2], Nobuteru Kubo[2], Hirofumi Shimada[2], Kota Torikai[2], Masami Torikoshi[2], Tatsuaki Kanai[2] and Takashi Nakano[2]

[1]Department of Radiation Oncology, Gunma University Graduate School of Medicine, 3-39-22 Showa-machi, Maebashi-shi, Gunma, 371-8511, Japan
[2]Gunma University Heavy Ion Medical Center, 3-39-22 Showa-machi, Maebashi-shi, Gunma, 371-8511, Japan
*Corresponding author. Department of Radiation Oncology, Gunma University Graduate School of Medicine, 3-39-22 Showa-machi, Maebashi-shi, Gunma, 371-8511, Japan. Tel: 027-220-8383; Fax: 027-220-8397; Email: masahr.kawa@gmail.com
(Received 20 July 2017; revised 30 October 2017; editorial decision 5 December 2018)

ABSTRACT

It is important to confirm the dose distribution and its biophysiological response in patients subjected to carbon-ion radiotherapy (CIRT) by using medical imaging methods. In this study, the correlation between the signal intensity changes of muscles observed in magnetic resonance imaging (MRI) after CIRT and planned dose distribution was evaluated. Seven patients were arbitrarily selected from among localized prostate cancer patients on whom CIRT was performed in our facilities in 2010. All subjects received the same dose of CIRT, namely, 57.6 Gy relative biological effectiveness (RBE) in 16 fractions. The following two types of images were acquired for each subject: planning computed tomography (CT) images overlaying the dose distribution of CIRT and MRI T2-weighted images (T2WI) taken 1 year after CIRT. The fusion image of the planning CT and MRI images was registered by using a treatment-planning system, and the CIRT dose distribution was compared with changes observed in the MRI of the obturator internus muscles located near the prostate. The signal changes in the axial image passing through the isocenter of the planning target volume were digitized, and a scatter diagram was created showing the relationship between the radiation dose and digitized signal changes. A strong correlation between the radiation dose and the MRI signal intensity changes was observed, and a quadratic function was found to have the best fit. However, estimating the dose distribution from the normalized MRI signal intensity is difficult at this point, owing to the wide variation. Therefore, further investigation is required.

Keywords: carbon-ion radiotherapy; magnetic resonance image; dose distribution; signal intensity changes

INTRODUCTION

Particle beam therapies, including carbon-ion radiotherapy (CIRT), are used, due to the expectation of clinical advantages for cancer treatment. Particle beams have a characteristic dose distribution called a Bragg peak, which makes it possible to reduce the dose to critical tumor-adjacent organs and to realize high dose concentration in the tumor, compared with photon beams [1]. In the comparison between the planned dose distribution and the change in the MRI signal after the carbon-ion radiotherapy, two types of uncertainties should be considered; one is the uncertainty due to geometrical factors, and another is the uncertainty of the biological response peculiar to carbon-ion radiotherapy. In the treatment planning for particle beam therapies, the particle beam penetration depth is calculated by using the CT number that is the attenuation coefficient of the diagnostic X-ray. It is well known that the conversion from CT number to stopping power may result in uncertainties in the dose distribution [2–4]. Body shape deformation, organ structure changes, and patient set-up errors occurring in fractionated daily radiation therapy affect the calculated stopping power and hence the actual dose distribution in the body. For these reasons, it is important to compare the planned prescribed dose distribution on CT images with the physiological response of the patient's tissue to the carbon-ion beam.

In photon therapy, it is possible to visualize the irradiation field by penetrating radiation using linac-graphy or megavoltage CT, and various studies concerned with the quality control of photon therapy have been conducted using this technique [5]. However, in particle therapy, images of penetrating radiation are unavailable due to the lack of penetrating particles; thus, it is difficult to perform dose distribution quality control by using the established dose distribution management technology in conventional photon therapy, and attempts have been made to use auto-activation PET (AA PET) as a technique for confirming the dose distribution in particle therapy *in vivo*. AA PET uses positrons produced *in vivo*. However, there is no validation of the relationship between PET images and dose distribution because it is difficult to perform accuracy analysis with a resolution of 2 mm or less as well as to analyze dose intensity [6]. In addition to that, attempts to confirm the irradiation field using biophysiological change due to irradiation have been attempted, but they are limited, and little has been established.

In the follow-up diagnostic magnetic resonance imaging (MRI) T2-weighted images (T2WI) of prostate cancer patients taken 1 year after carbon ion beam therapy, a high-signal area appeared in the internal obturator muscle near the prostate, which was almost consistent with the high-dose region near the end of the beam range [7]. In this study, the signal change and dose distribution in the treatment plan were considered by analyzing the correlation in the obturator muscle, and a method was proposed for confirming the dose distribution in the living body. Hence, the prescribed dose distribution was evaluated using MR images, which can indicate minute changes in tissue signal intensities induced by biophysiological changes caused by particle beam irradiation.

MATERIALS AND METHODS

Patients

Among the localized prostate cancer patients on whom carbon beam therapy was performed in our facilities from March to September 2010, seven patients who had MRI images of the prostate 1 year after the treatment were arbitrarily selected for this study. Their pelvic MRI for the treatment plan and the treatment plan CT, including dose distributions, were used for comparative analysis. This study was approved by the Institutional Review Board at Gunma University Hospital (Approval Number: 160026). The Clinical Trial Registration number was 160026.

The MRI images of seven cases before treatment and 1 year after treatment are shown in Supplementary Figure 1.

Treatment planning for CIRT

The feet of the patients were positioned in a customized cradle (Moldcare; Alocare, Tokyo, Japan), and the pelvis was immobilized in the supine position with a low-temperature thermoplastic sheet (Shellfitter; Keraray, Co., Ltd, Osaka, Japan), during both the planning CT and the actual treatment. In the CT simulation, the bladder was filled with 100 ml sterilized water and the rectum was emptied using an enema. The CT images for the treatment planning were taken in 2-mm slices by Aquilion LB (TOSHIBA Medical Systems, Otawara, Japan). The treatment planning system was XiO-N ver.4.4.7 (joint product of Elekta AB, Stockholm, Sweden and Mitsubishi Electric, Tokyo, Japan), and the calculation grid size was 2 mm × 2 mm × 2 mm. A radiation oncologist contoured the prostate and normal structures. The area including the prostate and the proximal seminal gland was defined as the clinical target volume (CTV), and a set-up margin of >5 mm (as per common practice) was added to CTV and was contoured as planning target volume (PTV). The rectum and bladder were contoured as organs at risk. Then a medical physicist optimized the treatment plan by calculating the dose distribution.

A total dose of 57.6 Gy (RBE)/16 fractions was prescribed. At first, doses of 32.4 Gy (RBE)/9 fractions were given with three beams from the frontal, left and right sides, and subsequently doses of 25.2 Gy (RBE)/7 fractions were given with with shrink lateral beams. Radiation technologists set the patient using the planned reference images and the orthogonal X-ray images based on bony structures [8, 9]. In addition, in the case of fractionation from the front, bladder infusion was performed to maintain bladder volume [10–12].

Image fusion and geometrical calibration

MRI 1 year after the start of the therapy was performed via MAGNETOM Avanto (SIEMENS Medical Systems, Erlangen, Germany). The imaging conditions were as follows. Magnetic field strength: 1.5–3 T, slice spacing: 3–4 mm, repetition time: 4000–4480 ms, echo time: 83–96 ms, field of view: 320 mm × 320 mm, matrix size: 1 mm × 1 mm × 2 mm. CT images of the treatment planning and T2WI 1 year after the start of the therapy were fused with reference to the bony structure on the XiO-N system. The units were changed from millimeters to pixels for analysis using the software package ImageJ 1.46r (Wayne Rasband, NIH, USA). The fused images in XiO-N, with a scale coordinate of 1 mm, were transferred to ImageJ.

Change in the prostate position and size before and after treatment

Prostate position and size changes were evaluated 1 year after the treatment, comparing the treatment planning of the prostate as well as the inner and outer lines of the obturator internus muscle. They were compared by measuring the distance from the isocenter point to the outer edge of the prostate in the axial plane, as well as the inner and outer edge of the inner obturator muscle along the isocenter line in all cases. Then, both distances were compared by using a paired *t*-test.

Planned dose vs MRI signal intensity

Using XiO-N, the position of the irradiation field was rigidly registered on the MRI images obtained 1 year after the treatment, and the CT images were rigidly registered mainly on the head of the femur and the pelvic bone. After the registration, the one-dimensional dose profile along the beam path in the left–right direction at the isocenter plane was extracted,. The doses on the horizontal isocenter line were plotted on the vertical axis against the horizontal distance on the isocenter line.

The fusion MRI images obtained 1 year after the treatment by XiO-N were displayed with a window width of 1000 and window

level of 400. In addition, the pixel value levels of the signal change of the internal obturator muscle were converted into 8-bit format in ImageJ. The pixel value level of the normal piriformis muscle was normalized calibrated as 0, and that of fat as 100. The signal change of the internal obturator muscle was expressed as a fraction of 100. The piriformis muscle used in normalized calibration is away from the irradiation field, so there is no signal change and it is the muscle depicted in the same slice. Regarding the fat area, subcutaneous fat on the ventral side of the same slice was adopted. The surroundings of the piriformis muscle and the subcutaneous fat were confirmed to some extent and the average pixel value in the area of a circle with a size of ~5 mm was used as a reference. The one-dimensional profile of the MRI signal intensity along the beam path in the left–right direction at the isocenter plane was extracted, and the values of MRI pixel intensity were plotted against the horizontal axis along the isocenter.

The extracted profiles of the planned dose and MRI intensity for each patient were compared in a scatter diagram. Furthermore, for each case, fitting was performed with a linear function, a quadratic function, and an exponential function, and the respective correlation coefficients R were obtained. A scatter plot with x- and y-axes representing the dose and normalized signal intensity level was obtained.

RESULTS

Changes in position before and after treatment of the prostate edge and the inner and outer edge of the obturator internus muscle are shown in Table 1. A t-test was performed, and no significant differences in these distances were found before and after CIRT. Figure 1 shows an example of MRI and planned CT images with dose distribution.

The MRI signal changes were in visual accordance with dose distribution. Figure 2 shows the curves of the normalized MRI signal intensity and the doses of the internal obturator muscle for the seven patients with prostate cancers treated with CIRT. The dose change in the observation area (average and standard deviation) was 2.68 ± 0.49 Gy (RBE) per 1 mm, and the MRI pixel values in the observation area were 3.91 ± 1.68 per 1 mm. Correlation between the gradient of MRI signal changes and the dose distribution of carbon beams was observed for all patients. Moreover, the intensity steepness of the MRI signal was well associated with that of dose distribution.

The correlations between the planned doses and MRI signal changes were analyzed based on the distance from the isocenters and are shown in Fig. 3. Table 2 shows the R values for each fitting function for all cases. Figure 4 shows the MRI pixel value corresponding to the dose distribution of each patient, and the regression curve of the quadratic function with the highest R. Table 3 also shows the coefficients when quadratic regression was performed so as to evaluate the correlation between MRI pixel value and radiation dose.

DISCUSSION

The anatomical structure of the internal obturator muscle near the prostate was not significantly changed 1 year after treatment, whereas the signal intensity of MRI increased. Hence, dose distribution and MRI structure could be superimposed well. The stage of the case was T1c–T3bN0M0, and irradiation field and dose did not change with the condition of the T stage. Therefore, in all cases, the condition of the irradiation field did not change with the stage. The present study indicates a significant correlation between the degree of MRI signal changes 1 year after the treatment and dose distribution of carbon beams for all patients. Moreover, the signal intensity was almost exponentially fitted to carbon beam irradiation doses. From Table 3, it can be seen that in the quadratic approximation

Table 1. The differences in the distance of the prostate and muscles edge from the isocenter

	Mean pre distance (mm)	Mean post distance (mm)	Mean difference (mm)	SD	*P* value
Prostate	34.66	33.59	−1.067	4.330	0.481
Inner line	50.98	52.16	1.178	3.471	0.338
Outer line	85.63	83.28	−2.356	3.874	0.106

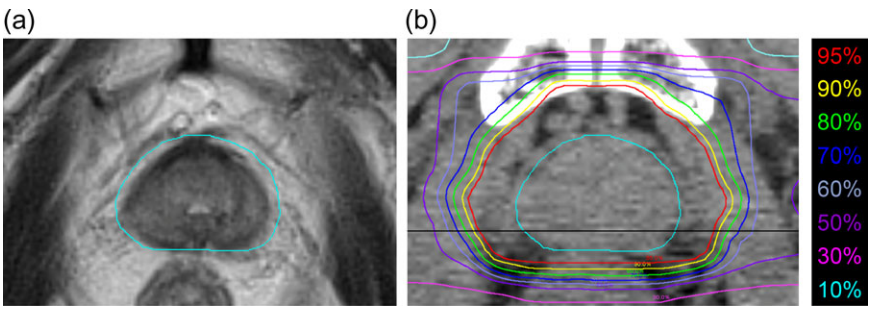

Fig. 1. Example of MRI and planned CT images. (a) T2-weighted MRI before treatment (b) CT images with dose distribution. Cyan lines show prostate, and black straight line shows the isocenter. MRI signal intensity and the dose were measured in the pixels of the muscle on the black line.

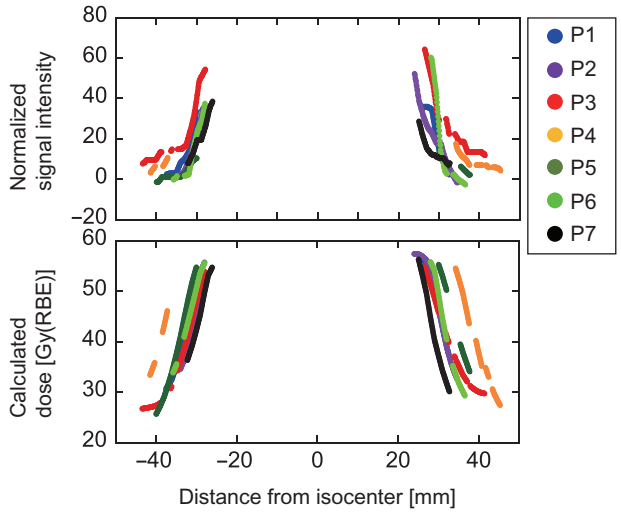

Fig. 2. Scatter diagram obtained by putting dose distribution and signal change for seven cases on the same coordinate axis.

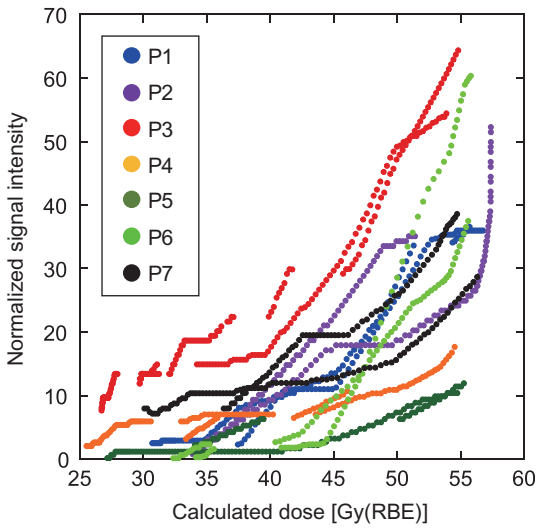

Fig. 3. Scatter diagram of distribution profile (*x*-axis) on the same coordinate axis and correlation of signal strength (*y*-axis) for all cases.

with the highest correlation, the average value of the second coefficient is 0.049, both of which are increasing functions. That is, for all patients, it can be seen that the MRI value increases as the dose increases.

However, as the standard deviation of the second coefficient is 0.046, and the variation among the patients is wide, it is difficult to uniquely identify the dose irradiated by using only the MRI pixel value.

Considering the dose and the MRI pixel value changes related to the deviation of the position [2.68 Gy (RBE) per 1 mm and 3.91 per 1 mm], the change of positional deviation due to dose and MRI pixel value is wide. However, the variation in the MRI pixel value among the patients is significantly larger than that for misregistration. For example, the maximum MRI pixel value of P 3 is 64.3 and the maximum value of P 5 is 12.0. For this reason, it is conceivable that causes other than the positional deviation are significantly related to the aforementioned variations in MRI change.

Recently, MRI has been used for the evaluation of the dose distribution in particle therapy *in vivo*. MRI has the most precise tissue resolution among the recent physiological imaging methods and may evaluate dose distribution more precisely than AA PET [13]. However, there are some uncertainties due to errors in this analysis as follows:

Geometrical uncertainty

- Conversion to stopping power ratio in dose calculation.
- Fusion of CT and MRI.
- MRI signal intensity.
- Artifacts of MR images.

Physiological uncertainty

- Tissue response to the high linear energy transfer (LET) radiation.

For dose calculation in particle beam therapy, conversion from the CT value to the stopping power ratio is performed. When the least squares method is used to estimate the stopping power from the CT value, ±0.82% of the statistical error is recognized, that is, an error of 3.28 mm at a depth of 200 mm in water [2].

In this analysis, the irradiation dose and the response by MRI were compared by using the CT image at the treatment plan and the MRI image after the treatment; however, as the MRI image was obtained 1 year after the CT image, there is a possibility that the

Table 2. The correlation coefficients (*R* values) between the radiation dose and the MRI signal intensity changes when fitting with the linear, quadratic and exponential functions for each patient are shown

Regression curve	1		2		3		4		5		6		7		Mean	SD
	Left	Right	Left	Right	Left	Right	Left	Right	Left	Right	Left	Right	Left	Right		
Linear	0.982	0.965	0.916	0.997	0.971	0.937	0.945	0.941	0.933	0.882	0.907	0.928	0.924	0.982	0.944	0.032
Quadratic	0.984	0.990	0.930	0.998	0.991	0.991	0.954	0.946	0.934	0.990	0.998	0.989	0.972	0.986	0.975	0.024
Exponential	0.958	0.971	0.937	0.951	0.992	0.985	0.959	0.948	0.938	0.980	0.986	0.945	0.960	0.986	0.964	0.019

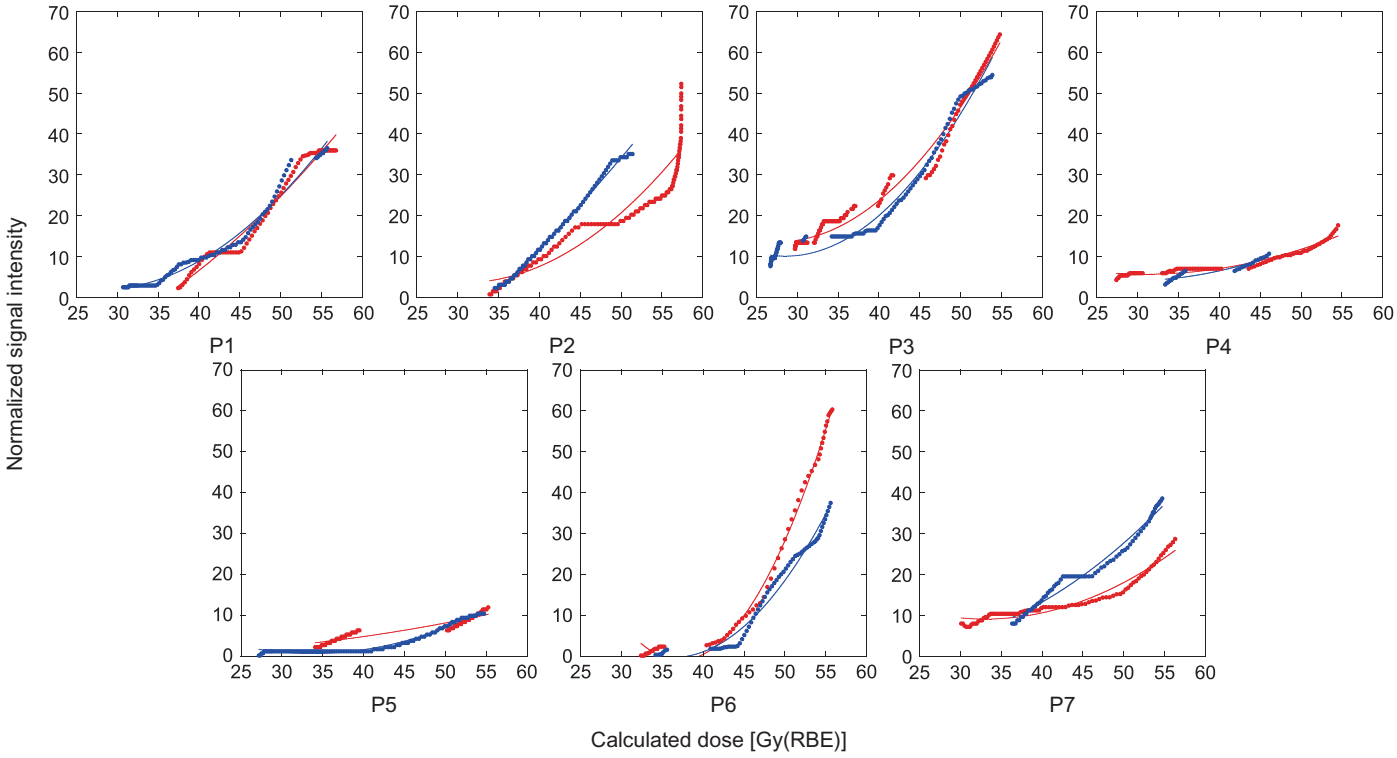

Fig. 4. Scatter diagram of dose distribution profile (*x*-axis) on the same coordinate axis, and correlation of signal strength (*y*-axis) for each case. The red points are on the left side, and the blue points are on the right side. The red and blue lines represent the quadratic approximation lines on the left and right side, respectively.

Table 3. The coefficients when fitting with a quadratic function for each patient ($y = a+bx+cx^2$) are shown

Coefficient	1		2		3		4		5		6		7		Mean	SD
	Left	Right	Left	Right	Left	Right	Left	Right	Left	Right	Left	Right	Left	Right		
a	−17.400	37.040	46.710	−48.710	64.111	71.911	20.649	20.486	0.965	27.645	244.760	132.130	42.860	16.670	47.131	70.985
b	−0.370	−2.550	−2.810	0.955	−3.653	−4.331	−1.035	−1.141	−0.094	−1.602	−13.222	−7.296	−2.047	−1.313	−2.894	3.608
c	0.024	0.046	0.046	0.014	0.066	0.076	0.017	0.020	0.005	0.024	0.178	0.105	0.031	0.031	0.049	0.046

internal position was different. Nevertheless, the reaction of the muscle near the bone structure can be seen, and thus this difference is considered to be small.

The response of MRI was not confirmed from the image before treatment, and the images after 2 years and after 1 year were compared, with the change clearly visualized in the image obtained 1 year after treatment. This MRI signal change is high intensity at T2WI and low intensity at T1WI, so it is considered to be an edematous inflammatory state, and the most clearly visualized time is unknown [14–16]. It is conceivable that differences in clarity between patients appear as errors in this analysis.

The MR image used now is influenced by distortion and cross-talk artifacts. However, these may hardly affect the result because it was confirmed that the distortion of the MRI image is <1 pixel from regular measurements made using a phantom.

In addition, differences in response due to the LET of the internal obturator muscle are unknown. In this study, the clinical dose, obtained by multiplying the physical dose and the RBE, was used for the analysis. Although the clinical dose of left and right muscle were nearly the same, the total LET of left or right muscle were different owing to the irradiation fractions from the left or right side. The current RBE would not show the muscle reaction correctly, although the RBE was calculated based on the human submandibular gland (HSG) cells [17]. It is assumed that left or right doses in Figs 2, 3 and 4 are slightly different. To evaluate *in vivo* muscle dosimetry, it is necessary to investigate the muscle reaction from the physical dose per LET.

At present, there are several restrictions on the method of confirming the dose distribution in particle beam therapy. In addition, as the difference in MRI pixel value among the patients is wide, it is difficult to use only the pixel value for confirming the dose distribution. However, this method can be performed only with MRI, which implies that there is no additional exposure compared, for instance, to AA PET, and that in view of directly verifying the muscle reaction, it has an advantage as a confirmation method.

Furthermore, the method proposed here might be useful for evaluating the clinical dose distribution and its physiological response in carbon-ion radiotherapy. That would be one of the clinical QA methods.

It was concluded that MRI signal intensity changes were correlated with CIRT dose distribution.

However, the estimation of the dose distribution from the normalized MRI signal intensity is difficult at this point, due to the wide variation. Hence, further investigation is required.

SUPPLEMENTARY DATA

Supplementary data are available at *Journal of Radiation Research* online.

CONFLICT OF INTEREST

The authors declare that there are no conflicts of interest associated with this manuscript.

FUNDING

None.

REFERENCES

1. Akakura K, Tsujii H, Morita S et al. Phase I/II clinical trials of carbon ion therapy for prostate cancer. *Prostate* 2004;58:252–8.
2. Matsufuji N, Tomura H, Futami Y et al. Relationship between CT number and electron density, scatter angle and nuclear reaction for hadron-therapy treatment planning. *Phys Med Biol* 1998;43:3261–75.
3. Lühr A, Toftegaard J, Kantemiris L et al. Stopping power for particle therapy: the generic library libdEdx and clinically relevant stopping-power ratios for light ions. *Int J Radiat Biol* 2012; 88:209–12.
4. Kubota Y, Kawamura H, Sakai M et al. Changes in rectal dose due to alterations in beam angles for setup uncertainty and range uncertainty in carbon-ion radiotherapy for prostate cancer. *PLoS One* 2016;11:1–11.
5. Mao W, Hsu A, Riaz N et al. Image-guided radiotherapy in near real time with intensity-modulated radiotherapy megavoltage treatment beam imaging. *Int J Radiat Oncol Biol Phys* 2009;75: 603–10.
6. Combs S, Bauer J, Unholtz D et al. Monitoring of patients treated with particle therapy using positron-emission-tomography (PET): the MIRANDA study. *BMC Cancer* 2012;12:133.
7. Chang JH, Lim Joon D, Nguyen BT et al. MRI scans significantly change target coverage decisions in radical radiotherapy for prostate cancer. *J Med Imaging Radiat Oncol* 2014;58:237–43.
8. Kubota Y, Tashiro M, Shinohara A et al. Development of an automatic evaluation method for patient positioning error. *J Appl Clin Med Phys* 2015;16:100–111.
9. Kubota Y, Hayashi H, Abe S et al. Evaluation of the accuracy and clinical practicality of a calculation system for patient positional displacement in carbon ion radiotherapy at five sites. *J Appl Clin Med Phys* 2018;19:144–53.
10. Ishikawa H, Tsuji H, Kamada T et al. Carbon ion radiation therapy for prostate cancer: results of a prospective phase II study. *Radiother Oncol* 2006;81:57–64.
11. Kumagai M, Okada T, Mori S et al. Evaluation of the dose variation for prostate heavy charged particle therapy using four-dimensional computed tomography. *J Radiat Res* 2013;54: 357–66.
12. Ishikawa H, Katoh H, Kaminuma T et al. Carbon-ion radiotherapy for prostate cancer: analysis of morbidities and change in health-related quality of life. *Anticancer Res* 2015;35:5559–66.
13. Gensheimer M, Yock T, Liebsch N et al. *In vivo* proton beam range verification using spine MRI changes. *Int J Radiat Oncol Biol Phys* 2010;78:268–75.
14. Messer JA, Mohamed AS, Hutcheson KA et al. Magnetic resonance imaging of swallowing-related structures in nasopharyngeal carcinoma patients receiving IMRT: longitudinal dose–response characterization of quantitative signal kinetics. *Radiather Oncol* 2016;118:315–22.
15. Nömayr A, Lell M, Sweeney R et al. MRI appearance of radiation-induced changes of normal cervical tissues. *Eur Radiol* 2001;11:1807–17.
16. May DA, Disler DG, Jones EA et al. Abnormal signal intensity in skeletal muscle at MR imaging: patterns, pearls, and pitfalls. *Radiographics* 2000;20 Spec No:S295–315.
17. Kanai T, Endo M, Minohara S et al. Biophysical characteristics of HIMAC clinical irradiation system for heavy-ion radiation therapy. *Int J Radiat Oncol Biol Phys* 1999;44:201–10.